Boundary-Layer Transition on a Film-Cooled Slender Cone

John Starkenberg* and Robert J. Cresci†
Polytechnic Institute of New York, Farmingdale, N.Y.

The research reported herein consists of a combined experimental and theoretical investigation of the downstream phenomena associated with the gaseous film cooling of a slender blunted cone in a hypersonic flow. A numerical solution of the boundary-layer equations with initial conditions reflecting mass injection is utilized to obtain predictions of the behavior of the downstream laminar boundary layer. Experimental measurements of heat transfer to the surface of the 10° half-angle cone model are made at a Mach number of 8, stagnation temperature of 2000°R, and freestream Reynolds numbers varying between 1×10^4 and 8×10^4/in. Comparison of the heat-transfer data with the theory indicates the existence of regions of nonlaminar flow over the surface of the model and has permitted identification of the point of onset of transition.

Nomenclature

$\bar{A}$ = minimum cross-sectional area of venturi
$\bar{c}_p$ = specific heat at constant pressure
$\bar{h}$ = enthalpy
M = Mach number
$\bar{m}_c$ = mass flow rate
Nu = Nusselt number
$\bar{p}$ = pressure
$\bar{q}$ = heat-transfer rate
$\bar{r}$ = radial coordinate from axis of symmetry
$\bar{R}_{\text{air}}$ = gas constant of air
$\bar{R}_I$ = interface radius
$\bar{R}_0$ = nose radius
$\bar{R}_s$ = shock radius
Re_∞ = freestream Reynolds number
Re_θ = local Reynolds number based on momentum thickness
$\bar{s}$ = tangential coordinate
$\bar{T}$ = temperature
$\bar{U}_\infty$ = freestream velocity
$\bar{u}$ = tangential velocity component
$\bar{v}$ = normal velocity component
$\bar{y}$ = normal coordinate
δ_c = cone half-angle
γ = ratio of specific heats
$\bar{\rho}$ = density
σ = Prandtl number
$\bar{\mu}$ = coefficient of viscosity

Subscripts

e = external flow condition
i = condition at end of injection region
0 = zero-injection condition
s = stagnation condition
tr = transition point condition
w = wall condition
∞ = freestream condition

Superscript

$-$ = dimensional quantity

Presented as Paper 75-194 at the AIAA 13th Aerospace Sciences Meeting, Pasadena, Calif., January 20-22, 1975; submitted January 29, 1975; revision received July 22, 1975. This research was supported by the Air Force Office of Scientific Research under Contract No. F44620-71-C-0008, Project No. 9781-01. This paper is taken from the dissertation submitted to the Faculty of the Polytechnic Institute of New York in partial fulfillment of the requirements for the degree of Doctor of Philosophy (Aeronautics and Astronautics), June 1975.

Index category: Boundary-Layer Stability and Transition.

*Research Assistant, Department of Aerospace Engineering and Applied Mechanics. Student Member, AIAA.

†Professor of Aerospace Engineering and Associate Provost for Research. Associate Fellow AIAA.

I. Introduction

INTEREST in the characteristics of the laminar and turbulent boundary layers on hypersonic vehicles with localized mass injection arises in connection with the problem of the thermal protection of these vehicles. It has been demonstrated amply that active mass injection systems may be required where presently available passive cooling techniques, such as surface ablation and heat sinks, are not feasible designs. This occurs, for example, on interplanetary re-entry vehicles, which necessarily travel at extremely high velocities and are characteristically slender with minimal blunting, as well as for atmospheric missiles, which require a stable aerodynamic shape for precise in-flight control. As a result, fairly detailed investigations of both film-cooling and transpiration-cooling techniques have been reported in the literature.

Although satisfactory surface cooling may be achieved by employing relatively small coolant mass flow rates distributed by transpiration cooling over a large region of the vehicle surface,[1-3] structural and functional limitations make the film-cooling technique the more attractive. The latter method is characterized by injection localized in a small region, generally in the neighborhood of the forward stagnation point. Coolant fluid may be injected through a porous medium covering the stagnation region or through a discrete slot, or series of discrete slots, slightly downstream of the stagnation point. Although differences in the effectiveness of the two techniques far downstream of the injection location should be negligible, the former method has the advantage of maximizing the local cooling effectiveness where the heat transfer is greatest.

Several effects of a fundamental fluid-dynamic nature arise in connection with the application of gaseous film cooling to a typical re-entry configuration, such as a slender cone with a slightly blunted nose including a porous injection region. These effects constitute the three principal areas of investigation in the present paper:

1) When the injection rate is sufficiently large, the inviscid flowfield may be altered in such a manner as to affect the shock shape and the pressure distribution on the cone surface. Cresci and Libby[4] have made use of an analysis based on

Lighthill's[16] constant-density solution for a sphere to predict the alteration of shock standoff distance with mass transfer. Conversely, it also was demonstrated experimentally that the inviscid flowfield remains essentially unchanged for sufficiently small injection rates. Martellucci and Laganelli[5] have suggested an empirical correlation involving an effective nose radius to predict the pressure distribution.

2) Reduction of the downstream heat transfer is the principal advantage of mass transfer cooling and has been the subject of the most extensive research. The essential features of the heat transfer when upstream mass injection is present have been studied by Libby and Cresci,[6] for example. They found that, where laminar flow prevails and at low rates of injection, the heat transfer is essentially that without injection except near the porous region, where it is significantly reduced. With increasing injection, the region of influence in the downstream direction progressively increases. This behavior is consistent with the parabolic nature of the boundary-layer equations and suggests the use of a numerical boundary-layer analysis with appropriate boundary conditions. The boundary layer may be considered in two distinct regions: the injection region and the downstream region. The former region may be modeled as a stagnation flow with mass transfer. The consequent analysis is well known and has been presented for homogeneous injection by Libby[7] and for foreign gas injection by Fox and Libby[8] and by Libby et al.,[9] among others. For the downstream region, the literature is much less abundant. The analyses of Cresci[10] and of Laganelli and Fogaroli[11] utilizing integral techniques have been employed to predict the heat-transfer distribution under conditions appropriate to the film cooling of re-entry configurations.

3) The destabilizing nature of upstream gas injection long has been recognized as leading to early boundary-layer transition on film-cooled surfaces. Cresci and Libby[6] and Dunavant and Everhart[12] have demonstrated that this effect may lead to higher heat-transfer rates with injection than without under certain conditions. Because of the decay in cooling effectiveness, laminar, film-cooled boundary layers exhibit a downstream increase in heat transfer to the surface. Since the onset of transition also is associated with a downstream increase in heat transfer, it generally is difficult to distinguish between the two effects. To date, there have not been available sufficient data to indicate the behavior of transition onset over a large range of Reynolds numbers.

The present investigation concerns itself with the downstream effects of gaseous, stagnation-point mass transfer at the nose of a slender cone. Heat-transfer measurements along the cone have been made over a range of mass flow rates and Reynolds numbers. In addition, an implicit, finite-difference technique has been used to predict the laminar boundary-layer behavior on the impermeable surface both with and without injection. Comparison of the results from the computer program with the experiments indicates the existence of regions of nonlaminar flow over the surface of the model and has permitted identification of the point of onset of transition.

II. Analysis of the Homogeneous Film-Cooled Boundary Layer

In order to analyze the complete problem of localized mass transfer into a hypersonic boundary layer, the flow is treated in two distinct regions, with the appropriate matching conditions at their junction. The upstream, stagnation, or injection region is characterized by its proximity to the forward stagnation point and by the presence of homogeneous injection at the wall. By far the most widely used analysis for flows of this type is the stagnation region similar solution as given by Libby.[7] However, it also is possible to make use of the inviscid, constant-density analysis of Cresci and Libby.[4]

The downstream region is characterized by the absence of injection at the wall and is amenable to analyses utilizing the integral technique or numerical integration of the full boundary-layer equations. Suitable initial conditions, which reflect the mass flow rate and introduce the effects of injection into the downstream analysis, are generated from the stagnation region analysis.

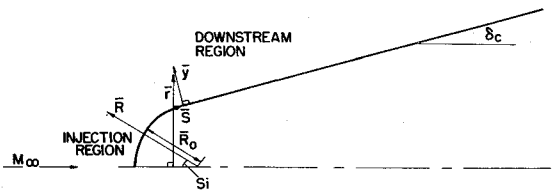

Fig. 1 Schematic of model coordinate system.

In the present case, the boundary-layer equations are integrated numerically downstream from the end of the injection region, making use of initial conditions obtained from either the stagnation region similar solution or the constant-density solution. Boundary conditions at the outer edge of the boundary layer are obtained from a knowledge of the external pressure distribution, assuming constant entropy and that the external flowfield remains unaltered by the injection.

The particular geometry and coordinate system under consideration is illustrated in Fig. 1. The body is a slender cone of half-angle δ_c with a spherically blunted nose of radius $\bar{R}_0$. The orthogonal curvilinear coordinates $\bar{s}$ *and* $\bar{y}$ are, respectively, tangential and normal to the body surface. The origin is located at the forward stagnation point.

A. Downstream Region

The various conservation equations, including the boundary-layer assumptions for axisymmetric flow, are given as follows:

Conservation of Mass

$$s\frac{\partial}{\partial s}(\rho u r)-\frac{\eta}{2}\frac{\partial}{\partial \eta}(\rho u r)+\frac{\partial}{\partial \eta}(\rho v r)=0$$

Conservation of Momentum

$$\rho u\left[s\frac{\partial u}{\partial s}-\frac{\eta}{2}\frac{\partial u}{\partial \eta}\right]+\rho v\frac{\partial u}{\partial \eta}+\frac{s}{\gamma M_\infty^2}\frac{dp}{ds}-\frac{1}{r}\frac{\partial}{\partial \eta}\left[\mu r\frac{\partial u}{\partial \eta}\right]=0$$

Conservation of Energy

$$\rho u\left[s\frac{\partial T}{\partial s}-\frac{\eta}{2}\frac{\partial T}{\partial \eta}\right]+\rho v\frac{\partial T}{\partial \eta}+(\gamma-1)\frac{p}{r}\left[s\frac{\partial}{\partial s}(ur)-\frac{\eta}{2}\frac{\partial}{\partial \eta}(ur)+\frac{\partial}{\partial \eta}(vr)\right]-\gamma(\gamma-1)M_\infty^2\left[\frac{\partial u}{\partial \eta}\right]^2-\frac{\gamma}{\sigma}\frac{\partial}{\partial \eta}\left[rc_p\mu\frac{\partial T}{\partial \eta}\right]=0$$

Equation of State

$$p=\rho T$$

where the following nondimensionalization has been introduced:

$$s=\bar{s}/\bar{R}_0 \qquad \eta=(Re_\infty/s)^{1/2}\bar{y}/\bar{R}_0 \qquad r=\bar{r}/\bar{R}_0$$

$$u=\bar{u}/\bar{u}_\infty \qquad v=(sRe_\infty)^{1/2}\bar{v}/\bar{U}_\infty \qquad p=\bar{p}/\bar{p}_\infty$$

$$T=\bar{T}/\bar{T}_\infty \qquad \rho=\bar{\rho}/\bar{\rho}_\infty \qquad \mu=\bar{\mu}/\bar{\mu}_\infty$$

$$c_p=\bar{c}_p/\bar{c}_{p\infty} \qquad h=\bar{h}/\bar{h}_\infty \qquad \sigma=\bar{c}_p\bar{\mu}/\bar{k}$$

$$Re_\infty=\bar{\rho}_\infty\bar{U}_\infty\bar{R}_0/\bar{\mu}_\infty$$

The finite-difference scheme employed here is that developed by Lin and Rubin[13] for flow over a sharp cone at moderate incidence. Their computer program has been modified to accept initial conditions reflecting upstream injection and to be applicable to general axisymmetric boundary-layer flows. Each term in the governing equations is replaced by a Crank-Nicholson difference quotient as specified by the predictor-corrector model of Rubin and Lin.[14]

B. Upstream Region

Two approaches are available for the solution of the upstream region, in which the mass transfer is present. These are described briefly in the following paragraphs.

Similar solutions

Following Lees,[15] the equations governing the axisymmetric stagnation point boundary layer become

$$(Cf'')'+ff''+\tfrac{1}{2}(t-f'^2)=0$$

$$(C\bar{c}_p t')'+\sigma\bar{c}_p f t'=0$$

where

$$C=\bar{\rho}\bar{\mu}/\bar{\rho}_e\bar{\mu}_e, \quad \bar{c}_p=\bar{c}_p/\bar{c}_{pe}$$

$$\bar{u}/\bar{u}_e=f'(\hat{\eta}), \quad \bar{T}/\bar{T}_e=\bar{\rho}_e/\bar{\rho}=t(\hat{\eta})$$

$$\hat{s}=\int_0^{\bar{s}}\bar{\rho}_e\bar{\mu}_e\bar{u}_e\bar{r}^2\,d\bar{s}\simeq\frac{1}{4}\bar{\rho}_e\mu_e\frac{d\bar{u}_e}{d\bar{s}}\bar{s}^4$$

$$\bar{\eta}=\frac{\rho_e u_e r}{(2\hat{s})^{1/2}}\int_0^{\bar{y}}\frac{\bar{\rho}}{\bar{\rho}_e}\,d\bar{y}\simeq\left\{\frac{2\bar{\rho}_e}{\bar{\mu}_e}\frac{d\bar{u}_e}{d\bar{s}}\right\}^{1/2}\int_0^{\bar{y}}\frac{\bar{\rho}}{\bar{\rho}_e}\,d\bar{y}$$

and primes indicate differentiation with respect to $\hat{\eta}$. The appropriate boundary conditions are

$$f'=0,\ f=f_w, \quad t=t_w \text{ at } \hat{\eta}=0$$

$$f'\to 1,\ t\to 1 \text{ for } \hat{\eta}\to\infty$$

Solutions to these equations subject to the preceding boundary conditions are useful for supplying initial conditions for the downstream integration when small mass flow rates are considered.

Isothermal shear layer

The results of a numerical integration of the foregoing equations indicate that for sufficiently large values of $-f_w$ the temperature and shear remain essentially unchanged in a thin layer near the wall. That is, $t=t_w$, $G=G_w$ where $G=Cf''$. This layer accordingly is referred to as the isothermal shear layer wherein the following relations also are valid:

$$u/u_e\simeq(s_i\rho_e\beta_{s_e}/2\mu_e)^{1/2}[\eta/(-f_w)] \tag{1}$$

$$m_c\simeq(2Re_\infty\rho_{s_e}\mu_{s_e}\beta_{s_e})^{1/2}\pi s_i^2\bar{\mu}_\infty\bar{R}_0(-f_w) \tag{2}$$

with

$$\beta_{se}=(du_e/ds)_s$$

Introducing the injection parameter

$$N_c=\bar{m}_c/\bar{\mu}_\infty\bar{R}_0\rho_{se}\beta_{se}Re_\infty^{1/2}$$

and eliminating $-f_w$ between Eqs. (1) and (2) results in the following expression:

$$u/u_e\simeq\pi s_i^{5/2}(\eta/N_c) \tag{3}$$

Constant-density solution

The constant-density solution as employed by Cresci and Libby[4] to predict shock standoff distance has been adapted to provide initial conditions for the downstream numerical integration. A spherical shock of radius $\bar{R}_s$ is associated with a sphere of radius $\bar{R}_0$. The flow between the bow shock and the body is divided into two layers separated by a spherical interface of radius $\bar{R}_I$. The outer layer consists of fluid passing through the shock from upstream infinity. The inner layer consists of injected fluid. Both regions are treated as axisymmetric, incompressible, rotational flows. Continuity of pressure and radial velocity is enforced at the interface.

The application of the foregoing analysis leads to the following expressions for the tangential velocity and mass flow:

$$u=\frac{2t_w^{1/2}u_e}{(2R_I^2+10R_I^{-1}-12R_I^{-3})}[2(2R_I^{-3}+1)R^3-(4R_I^{-3}+R_I^2)R-(2-R_I^2)R^{-2}] \tag{4}$$

$$m_c=2\pi\sin(s_i)\bar{\mu}_\infty\bar{R}_0Re_\infty t_w^{1/2}u_e(s_i)\rho_{s_e}\left[\frac{(5-3R_I^2-2R_I^3)}{(2R_I^2+10R_I^{-1}-12R_I^{-3})}\right]$$

Then

$$N_c=2\pi u_e(s_i)\sin(s_i)\left[\frac{(Re_\infty t_w)^{1/2}}{du_e/ds}\right]\left[\frac{(5-3R_I^2-2R_I^3)}{(2R_I^2+10R_I^{-1}-12R_I^{-3})}\right] \tag{5}$$

The results of the stagnation region similar solution and the constant-density solution may be compared when the assumptions of both theories apply; i.e., for the similar solution, the effects of viscosity must be minimal, and the constant-density solution must be restricted to thin layers. In order to accomplish this, it is necessary to restrict the results of the constant-density analysis to the case of thin layers by employing the following approximations:

$$R_I=1+\delta_I \quad \delta_I<<1$$

$$R=1+\delta_2 \quad \delta_2<<1$$

where

$$\delta_2=\bar{y}/\bar{R}_0=(s_i/Re_\infty)^{1/2}\eta$$

Eq. (4) then yields

$$u/u_e\simeq t_w^{1/2}(s_i/Re_\infty)^{1/2}(\eta/\delta_I) \tag{6}$$

and from Eq. (5) there results

$$N_c\simeq\pi s_i^2(Re_\infty/t_w)^{1/2}\delta_I \tag{7}$$

Eliminating δ_I between Eqs. (6) and (7) yields

$$u/u_e\simeq\pi s_I^{5/2}(\eta/N_c)$$

which is identical to Eq. (3). The value of η at the interface then is given by

$$\eta_I=t_w^{1/2}N_c/\pi s_I^{5/2}$$

The discontinuity occurring at the interface may be smoothed as follows in order to account for the effects of viscosity:

$$U_i(\eta) = u_e(s_i) \begin{cases} \dfrac{\pi s_i^{5/2}}{N_c}\,\eta & \eta \le \eta_l - \alpha \\ 1 - \left[1 - \dfrac{\pi s_i^{5/2}}{N_c}\,\eta\right] \exp\{-a[\eta - (\eta_l - \alpha)]^n\} & \eta \ge \eta_l - \alpha \end{cases}$$

$$T_i(\eta) = T_e(s_i) \begin{cases} t_w & \eta \le \eta_l - \alpha \\ 1 - (1 - t_w)\exp\{b[\eta - (\eta_l - \alpha)]^n\} & \eta \ge \eta_l - \alpha \end{cases}$$

where

$$a = [1/(2\alpha)^n]\ \ln\{x[1 - (\pi s_l^{5/2}/N_c)(\eta_l + \alpha)]\}$$

$$b = [1/(2\alpha)^n]\ \ln[z(1 - t_w)]$$

Comparison with the corresponding similar solution has been used to determine the numerical constants: $\alpha = 3.5$, $n = 4$m $x = 1000$, and $z = 200$. The foregoing profiles thus are placed in a form suitable for use as initial conditions for the integration of the boundary-layer equations in the downstream region.

III. Description of Experiments

All tests were conducted in the hypersonic wind tunnel at the Polytechnic Institute of New York, Aerodynamics Laboratory. The tunnel is of the intermittent type, operating at a nominal Mach number of 8. The stagnation pressure was varied from 50 to 400 psia corresponding to Reynolds numbers varying from 1×10^4 to 8×10^4/in. The stagnation temperature was maintained at approximately 2000°R, and the model surface to stagnation temperature ratio accordingly was equal to 0.275. For the injection tests, coolant mass flow rates varied up to 1.1×10^{-4} slug/sec.

The heat-transfer model, illustrated in Fig. 2, is a 10° half-angle cone with a spherically blunted nose of radius $\bar{R}_0 = 0.5$ in. The spherical nose includes a porous plug coined from a flat sheet of sintered stainless-steel powder, subtending a total angle of 60°. The entire nose section is threaded and removable to permit replacement of the porous plug without removing the model from the tunnel. A spacing gasket placed between the plug and the nose section is used to assure a smooth transition from the porous to the impermeable surface. A solid stainless-steel plug and a similar one with a pressure tap at the stagnation point were constructed for use during the zero-injection tests. The walls of the conical afterbody are approximately 0.070 in. thick. The model surface is instrumented with 26 thermocouples along one meridian and five pressure taps along another. The settling chamber behind the porous plug is instrumented with a pressure tap and an open-tip thermocouple for measuring coolant conditions prior to injection.

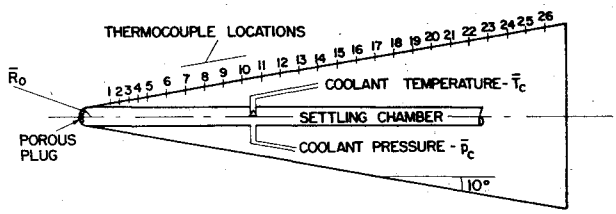

T.C.#	1	2	3	4	5	6	7	8	9	10	11	12	13
S	3.4	4.4	5.4	6.4	7.4	9.4	11.4	13.4	15.4	17.4	19.4	21.4	23.4

T.C.#	14	15	16	17	18	19	20	21	22	23	24	25	26
S	25.4	27.4	29.4	31.4	33.4	35.4	37.4	39.4	41.4	43.4	45.4	47.4	49.4

Fig. 2 Model design and instrumentation.

It should be noted that a high pressure drop across the porous plug must be maintained, since a high pressure but low flow rate is required in the settling chamber. This is necessary in order to prevent inflow through the plug in the neighborhood of the stagnation point. When the pressure in the settling chamber is sufficiently high, variations in the external pressure over the porous surface are negligible, and the outflow is uniform.

Air is supplied to the settling chamber from a high-pressure source through a regulator, a needle valve, a venturi flowmeter, and a shutoff valve, in that order. The coolant mass flow rate $\dot{m}_c$ is related to the venturi pressure drop $\Delta\bar{p}$, settling chamber pressure $\bar{p}_c$ and temperature $\bar{T}_c$ as follows:

$$\dot{m}_c = \bar{A}\bar{p}_c \left\{ \frac{2\gamma}{(\gamma - 1)\bar{R}_{\text{air}}\bar{T}_c} \left[\left[1 - \frac{\Delta\bar{p}}{\bar{p}_c} \right]^{2/\gamma} - \left[1 - \frac{\Delta\bar{p}}{\bar{p}_c} \right]^{(\gamma+1)/\gamma} \right] \right\}^{1/2}$$

where $\bar{A}$ is the minimum cross-sectional area of the venturi. The settling chamber pressure and the venturi pressure drop are measured with differential transducers, whereas the temperature $\bar{T}_c$ is measured by the open-tip thermocouple. All of these data were recorded during the tests.

Heat-transfer data were obtained from iron-constantan thermocouples. Between tests, the regulator in the coolant supply system was adjusted to a level that would permit precise setting of the needle valve to a desired flow rate. The shutoff valve was opened, and the needle valve was set using the value of $\bar{p}_c$ as a guide. The shutoff valve then was closed until immediately prior to the test, when it again was opened. The $\bar{p}_c$ and $\Delta\bar{p}$ readings were permitted to stabilize, and the test was run. The thermocouple output was recorded on single-channel recording potentiometers. A transient technique was used to determine the heat transfer, with an essentially uniform model temperature taken to be equal to the coolant temperature in the settling chamber ($\bar{T}_w = \bar{T}_c$). In order to prevent overheating of the model, test times were kept to a minimum. The model was polished periodically to counter the adverse effects of surface roughness caused by erosion. The recorded thermocouple output was tabulated in millivolts per second and reduced to heat-transfer rates and Nusselt numbers by the Wang 2200 computer, with the Nusselt number given by

$$Nu = \bar{q}\bar{R}_0\bar{c}_{p_\infty} / [(\bar{h}_\infty - \bar{c}_{p_w}\bar{T}_w)\bar{k}_\infty]$$

IV. Results and Discussion

It should be noted that the heat transfer (Nusselt number) is the dependent variable in this problem and as such depends on three independent variables: freestream Reynolds number, mass flow rate, and downstream distance. The first of these is a well-known similarity parameter, and the third describes geometric similarity. Particular attention is directed toward the effects of mass flow. Thus it becomes necessary to reduce the heat-transfer data to a form that is independent of Reynolds number in order to eliminate this as a parameter. This is possible for laminar flows for which the Nusselt num-

ber varies as the square root of the Reynolds number. However, rather than present data in the form of $Nu/Re_\infty^{\frac{1}{2}}$ for flows with injection, they are presented in the form of Nusselt numbers normalized with respect to their corresponding zero-injection values (Nu/Nu_0). Since the zero-injection Nusselt numbers correspond to laminar flow and hence to the associated Reynolds number dependence, the normalized Nusselt number will remain independent of Reynolds number as long as laminar flow prevails on the film-cooled surface. This means, for laminar flows, that all variations in normalized Nusselt number must be due to the effects of the other two independent variables, i.e., upstream mass addition and downstream distance. Comparison of data over the range of Reynolds numbers considered herein then becomes possible when the appropriate mass flow similarity parameter is selected.

The Reynolds number is a well-known similarity parameter reflecting the relative effects of the inertial and viscous forces. A similarity parameter reflecting the effects of injection also is required. The injection parameter N_c was introduced for the upstream analysis, but it remains to be determined whether it is the appropriate similarity parameter in the downstream region. It is possible to verify experimentally that this is the case based on examination of the heat-transfer data taken at small values of the mass flow rate. Figure 3 illustrates the experimental and theoretical variation of normalized Nusselt number with downstream distance s for various pairs of Reynolds numbers at several small values of N_c for which the boundary layer remained laminar. The close agreement between the data taken at different Reynolds numbers and the theory supports the contention that the parameter N_c alone reflects the effects of injection over the entire range of Reynolds numbers in a laminar flow.

For laminar flows, consideration of the normalized Nusselt number eliminates Reynolds number effects. In order to focus on the effects of injection, a single thermocouple location may be considered, thus eliminating the effects of geometry. The manner in which the injection affects the heat transfer to a point on the model is illustrated in Fig. 4, in which Nu/Nu_0 is plotted as a function of N_c at $s = 19.4$. Data for all Reynolds numbers at which tests were run are included. Typically, as N_c increases, the heat transfer to the surface is reduced in agreement with the theory until a point is reached at which the data begin to diverge from the theory, indicating the inception of transitional flow. Throughout the transition region, the heat transfer continues to increase with increasing injection, and then decreases when fully turbulent flow is achieved. The figure also indicates one effect of Reynolds number, i.e., that the departure from laminar flow occurs at smaller values of the injection parameter for higher Reynolds numbers.

When nonlaminar flow occurs, the Reynolds number dependence of the Nusselt number is no longer the same as at zero injection. This means that transitional or fully turbulent heat-transfer data presented in the form of normalized Nusselt numbers will exhibit a divergence from the laminar theory and from the transitional or fully turbulent data taken at other Reynolds numbers. This point is well illustrated in Fig. 5, which shows the downstream distribution of normalized Nusselt number for several values of the Reynolds

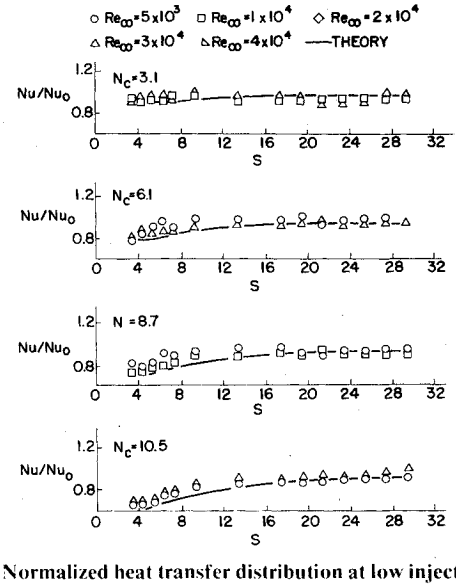

Fig. 3 Normalized heat transfer distribution at low injection rates.

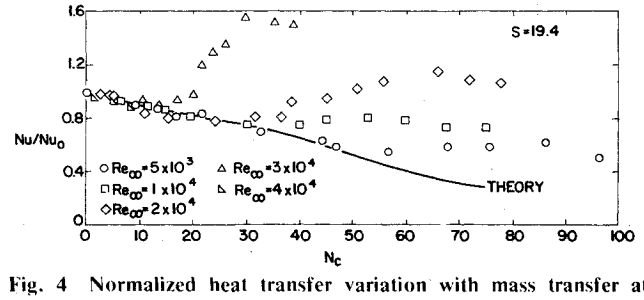

Fig. 4 Normalized heat transfer variation with mass transfer at $S = 19.4$.

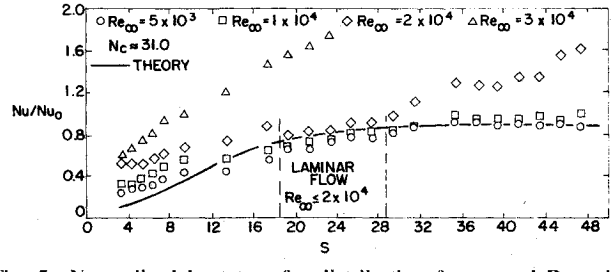

Fig. 5 Normalized heat transfer distribution for several Reynolds numbers at $N_c = 31.0$.

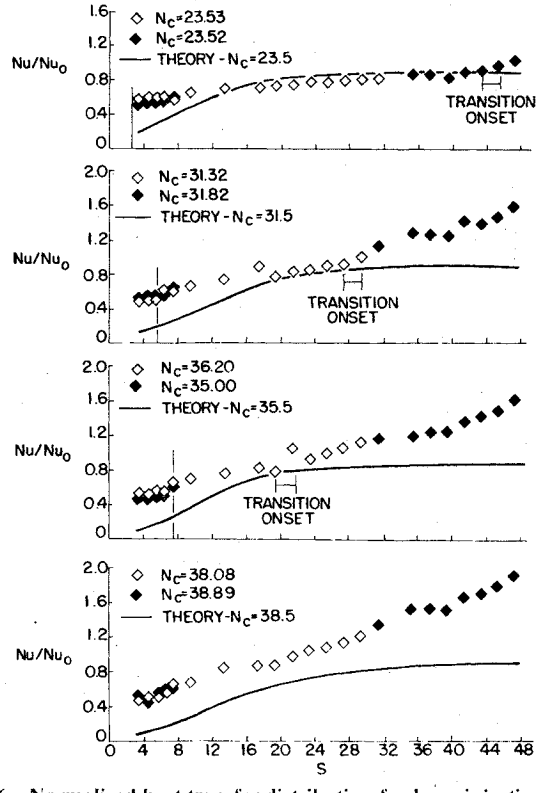

Fig. 6 Normalized heat transfer distribution for large injection rates at $R_{e_\infty} = 2 \times 10^4$.

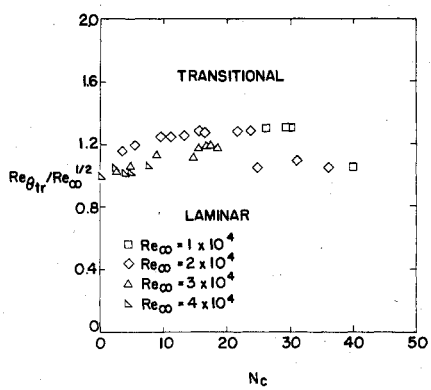

Fig. 7 Experimental location of transition.

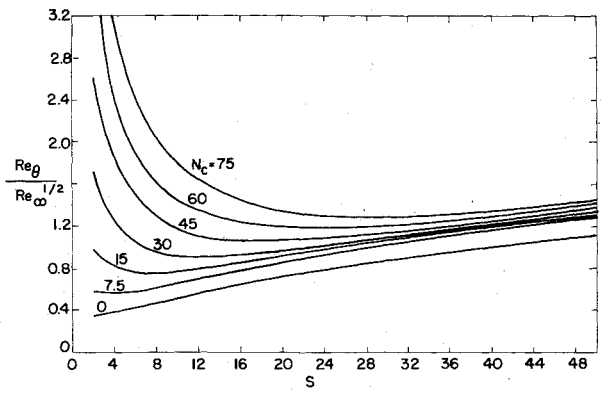

Fig. 8 Theoretical variation of $R_{c\theta}$.

number at $N_c \simeq 31$. Examining the data, such a divergence may be observed both upstream and downstream of a central region wherein the flow is laminar. For the two smaller Reynolds numbers, laminar flow also persists into the upstream and downstream regions. The most striking feature noticed in this figure is the presence of an upstream region of apparently nonlaminar flow and the subsequent downstream relaminarization of the boundary layer.

Figure 6 illustrates typical behavior of the data with increasing injection. Generally the boundary layer is laminar over the entire length of the model at sufficiently small Reynolds numbers and mass flow rates. As the Reynolds number or mass flow increases, nonlaminar flow first appears on the upstream portion of the body. The flow then relaminarizes at some point downstream. Transition from laminar to turbulent flow on the aft portion of the model may occur, depending on the Reynolds number and on the value of N_c.

Where possible, transition onset has been identified on the plots in Fig. 6 as the point at which the data first begin to diverge from the theory. The point of onset of transition is observed to depend on the freestream Reynolds number and on the injection parameter. The effects of these two parameters are reflected in the local Reynolds number based on momentum thickness Re_θ. Figure 7 summarizes the transition data on a plot of the transition value of the local Reynolds number divided by the square root of the freestream Reynolds number vs injection parameter. For values of the ordinate falling below the data, laminar flow prevails. This behavior is consistent with the concept that transition occurs due to instabilities created by thickening of the boundary layer.

The presence of the upstream disagreement with theory is subject to various interpretations. Among the most plausible are that the boundary layer is unstable due to the considerable thickening that occurs in the upstream region when injection is present or that the external flowfield is altered by the injection in such a manner as to produce increased pressure on the cone surface, resulting in higher laminar heat-transfer rates. In order to rule out this latter effect, pressure measurements were made on the cone model with injection. The results indicate no significant pressure alteration, consistent with the assumption that the injection does not alter the external flowfield. The manner in which the local Reynolds number based on momentum thickness behaves is illustrated in Fig. 8. For flows without injection, Re_θ is a monotonically increasing function of downstream distance. Transition is observed to occur when this parameter becomes sufficiently large at some point downstream. When injection is present, the boundary layer is significantly thickened in the upstream region so that the conditions required for the existence of laminar flow may not be satisfied. The local Reynolds number is no longer monotonic but decays asymptotically to the zero-injection behavior downstream. In some cases, Re_θ may become sufficiently small to permit relaminarization of the boundary layer.

The observed behavior of the homogeneous film-cooled boundary layer may be described in terms of the foregoing interpretation. Particular attention is drawn to Figs. 3 and 6, which exemplify this behavior. For $3.5 \leq N_c \leq 10.0$, incipient transition appears near the aft end of the model, whereas the upstream region remains laminar. Nonlaminar flow on the upstream portion of the model appears for $N_c \geq 13$. With increasing injection, the transition point moves forward while the relaminarization point moves rearward, precipitating the merger of the two nonlaminar regions for $35.5 \leq N_c \leq 38.5$. At lower Reynolds numbers, the upstream region of nonlaminar flow appears alone. Incipient downstream transition is observed for $Re_\infty = 1 \times 10^4$, whereas no transition onset is observed for $Re_\infty = 5 \times 10^3$.

Based on the criterion developed for the downstream onset of transition (Fig. 7), it is possible to determine for each Reynolds number and value of N_c a value of s which corresponds to the point at which Re_θ first becomes small enough to permit relaminarization. These values of s are indicated in the plots in Fig. 6 by vertical lines. As may be expected, the boundary layer does not relaminarize immediately; rather, the nonlaminar flow persists for some distance downstream until all fluctuations are damped out.

V. Conclusions

The research reported herein consisted of an experimental and theoretical investigation of the downstream phenomena associated with the gaseous film cooling of a slender blunted cone in a hypersonic flow. The principal results achieved may be summarized as follows. The mass flow similarity parameter N_c, suggested by the stagnation region analysis, was shown to be applicable to the downstream region. Comparison of the heat-transfer data and the theory indicated the existence of regions of nonlaminar flow on the model. The downstream nonlaminar region was attributed to the onset of transition. The upstream nonlaminar region also is attributed to the appearance of instabilities induced by the considerable thickening of the boundary layer in the upstream region in the presence of injection.

It was possible to obtain a correlation including the effects of Reynolds number and mass flow which offered a uniform criterion for the onset of transition at all Reynolds numbers. From this correlation, it then was possible to determine the point on the model at which the conditions appropriate to laminar flow first appear with increasing s and to compare this with experimentally observed relaminarization. The flow always was observed to relaminarize downstream of this point, consistent with the behavior to be expected.

References

[1] Low, G.M., "The Compressible Laminar Boundary Layer with Fluid Injection," NACA TN 3404, March 1955.

[2] Pappas, C.C. and Okuno, A.F., "Measurement of Heat Transfer and Recovery Factor of a Compressible Turbulent Boundary Layer on

a Sharp Cone with Foreign Gas Injection," NASA TN D-2230, April 1964.

[3]Helenbrook, R.G., McConarty, W.A., and Anthony, F.M., "Evaluation of Active Cooling Systems for a Mach 6 Hypersonic Transport Airframe," NASA CR-1917, Dec. 1971.

[4]Cresci, R.J. and Libby, P.A., "The Downtream Influence of Mass Transfer at the Nose of a Slender Cone," *Journal of Aerospace Sciences*, Vol. 29, No. 7, July 1962.

[5]Martellucci, A. and Laganelli, A., "Downstream Effects of Gaseous Injection through a Porous Nose," Tech. Info. Ser. 71SD218, Feb. 1971, General Electric Co.

[6]Libby, P.A. and Cresci, R.J., "Experimental Investigation of the Downstream Influence of Stagnation-Point Mass Transfer," *Journal of Aerospace Sciences*, Vol. 28, No. 1, Jan. 1961.

[7]Libby, P.A., "The Homogeneous Boundary Layer at an Axisymmetric Stagnation Point with Large Rates of Injection," *Journal of Aerospace Sciences*, Vol. 29, No. 1, Jan. 1962.

[8]Fox, H. and Libby, P.A., "Helium injection into the Boundary Layer at an Axisymmetric Stagnation Point," *Journal of Aerospace Sciences*, Vol. 29, No. 8, Aug. 1962.

[9]Libby, P.A., Cresci, R.J. and Fox, H., "Studies of the Effects of Mass Transfer at a Stagnation Point," *presented at the American Rocket Society Space Flight Report to the Nation,* held at the New York Coliseum, Oct. 9-15, 1961, ARS Paper No. 2170-61.

[10]Cresci, R.J., "Theoretical Analysis of the Downstream Influence of Mass Transfer in a Stagnation Region," *International Journal of Heat and Mass Transfer*, Vol. 5, Sept. 1962, pp. 837-857.

[13]Lin, T.C. and Rubin, S.G., "Viscous Flow Over a Cone. Part 2. Supersonic Boundary Layer," *Journal of Fluid Mechanics*, Vol. 59, pt. 3, July 1973, pp. 593-620.

[14]Rubin, S.G. and Lin, T.C., "A Numerical Method for Three-Dimensional Viscous Flow: Application to the Hypersonic Leading Edge," *Journal of Computational Physics,* Vol. 2, April 1972, pp. 339-364.

[15]Lees, L., "Laminar Heat Transfer Over Blunt-Nosed Bodies at Hypersonic Flight Speeds," *Jet Propulsion,* Vol. 26, No. 4, April 1956, pp. 259-269.

[16]Lighthill, M.J., "Dynamics of a Dissociating Gas," *Journal of Fluid Mechanics*, Vol. 2, Jan. 1957, pp. 1-32.

From the AIAA Progress in Astronautics and Aeronautics Series . . .

THERMAL POLLUTION ANALYSIS—v. 36

Edited by Joseph A. Schetz, Virginia Polytechnic Institute and State University

This volume presents seventeen papers concerned with the state-of-the-art in dealing with the unnatural heating of waterways by industrial discharges, principally condenser cooling water attendant to electric power generation. The term "pollution" is used advisedly in this instance, since such heating of a waterway is not always necessarily detrimental. It is, however, true that the process is usually harmful, and thus the term has come into general use to describe the problem under consideration.

The magnitude of the Btu per hour so discharged into the waterways of the United States is astronomical. Although the temperature difference between the water received and that discharged seems small, it can strongly affect its biological system. And the general public often has a distorted view of the laws of thermodynamics and the causes of such heat rejection. This volume aims to provide a status report on the development of predictive analyses for temperature patterns in waterways with heated discharges, and to provide a concise reference work for those who wish to enter the field or need to use the results of such studies.

The papers range over a wide area of theory and practice, from theoretical mixing and system simulation to actual field measurements in real-time operations.

304 pp., 6 x 9, illus. $9.60 Mem. $16.00 List

TO ORDER WRITE: Publications Dept., AIAA, 1290 Avenue of the Americas, New York, N. Y. 10019